



Effects of Grain-Size Composition Examined in Laboratory and Numerical Tests on Artificial Mud-Flows

Simonetta Cola, Nancy Calabrò, Paolo Simonini, and Manuel Pastor

Abstract

This paper deals with a laboratory and numerical research on mudflows performed in with the aim to study the interrelations between the grain-size composition of the mud and its rheological properties at different solid concentrations. Furthermore, the predicting capability of a new numerical model in reproducing the flow of viscous materials is evaluated.

Keywords

Mudflows • Viscous materials • Run-out model • Grain-size composition

Introduction

Mudflows, or more generally earth-flows, represent a permanent hazard in large part of Italian territory. A clear understanding of these phenomena is required to analyse landslides risk and to optimize slope stabilisation strategies. The risk strictly depends on the run-out, magnitude and displacement rate of mudflows. Particularly, the rate, ranging between some mm/y and some tens of m/s, is the key factor for risk assessment.

The distinctive features of mudflow are related to the slope morphology and the physical and rheological properties of the involved materials, which are responsible for their long travel distances (up to tens of kilometres) and the high velocities they may attain. Among these factors, the most relevant are the geotechnical soil properties (water content, grain size, plasticity properties, etc.).

In the last 20 years, researchers have developed a number of new sophisticated numerical models for the propagation prediction in the framework of the continuum and discrete element mechanics. These models hypothesis that for many

flow-like landslides the average depths are small in comparison with their length or width: in these conditions it is possible to simplify the 3D propagation model by integrating its equations along the vertical axis. The resulting 2D depth-integrated model presents an excellent combination of accuracy and simplicity, providing information about propagation, such as velocity or depth of the flow along the path. For instance, Hutter and his co-workers (Savage and Hutter 1991; Hutter and Koch 1991) or Laigle and Coussot (1997) have successfully used some depth-integrated models to model flow-like landslides.

Recently, Cola et al. (2008) analysed the propagation of Tessina earth-flow (Fig. 1) with a depth-integrated SPH model (pastor et al. 2008). This model integrates a 2D propagation model with the method of *Smoothed Particle Hydro-dynamics*, SPH, a new integration approach separately proposed by Lucy (1977) and Gingold and Monaghan (1977).

In their work, Cola et al. described the rheological behavior of the soil involved in Tessina earth-flow by means of the Bingham model, with parameters calibrated on tests performed on the soil fine fraction only. They evidenced the important role played by the viscosity on the predicted propagation and the need for rheological parameters calibrated on the behavior of entire soil for a more reliable prediction of real events. At the same time, they showed the importance of checking the numerical

S. Cola (✉) • N. Calabrò • P. Simonini
Università di Padova, Dip. Image, Via Ognissanti 39, 35129 Padova,
Italy
e-mail: simonetta.cola@unipd.it

M. Pastor
Politécnica de Madrid, Madrid, Spain



Fig. 1 View of Tessina landslide and sampling location

model reliability on the base of well-documented flow phenomena, condition seldom if ever verified.

Tests on small-scale physical model represent an alternative powerful tool for investigating the mudflow behaviour in controlled conditions, allowing high precision monitoring of important features, such as the advancing rate of the mud wave or the thickness of the tongue, and, at the same time, permitting to evaluate the influence of soil properties on the propagation process. Finally, the knowledge gained by laboratory tests may be used to validate, improve and calibrate numerical models describing this kind of phenomena.

This paper describes an experimental research carried out at the University of Padova on small artificial mudflows and the following calibration activity for the assessment of the new SPH model.

Testing Program

Experimental tests were performed on three remoulded samples obtained from material collected at the toe of the large Tessina mudflow (Belluno, Italy), along the closing channel near Funes village (Fig. 1).

The in-situ material originates from the alteration of in-situ rocks, mainly Flysch rock composed by alternating layers of hard limestone and weak siltstone. This is evident from the grain-size curve (Fig. 2) showing two distinct portions within the majority of soil gathers: a coarse fraction, constituted by limestone fragments and retained on n.40 ASTM sieve, and the remaining fine fraction, originated from the breaking up of the highest silt content layers. The fine fraction, or matrix, is medium-low plasticity inorganic clay with average liquid and plastic limits equal to 39 and 19 respectively.

The rheological behaviour of the fine fraction was investigated by means of tests with the FANN V-G

rheometer, determining the shear stress in steady state condition at 300 and 600 r/min, and interpreting the readings with the Bingham law. The Bingham viscosity μ_b and the yield strength τ_c were determined for a solid concentration varying from 20 % to 35 % (Fig. 3). According to previous researches (O'Brien and Julien 1988; Major and Pierson 1992; Coussot and Piau 1994), μ_b and τ_c depend on solid concentration by exponential laws, which, in this case, turn out to be as follows:

$$\tau_c = 0.268e^{17.5c_v} \quad (1)$$

$$\mu_b = 5.6 \cdot 10^{-4} e^{12.7c_v} \quad (2)$$

with the solid concentration c_v defined as:

$$c_v = \frac{V_s}{V_T} \cdot 100 = \frac{1}{1 + G_S W} \quad (3)$$

being V_s the solid fraction volume, V_T the total volume of the sample, G_S the specific gravity of the soil particles and W the water content.

In the narrow analyzed range, the yield strength and plastic viscosity vary significantly, rising from 10 to 140 Pa and from 0.002 to 0.08 Pa·s respectively.

Two rectangular metallic planes (50 × 100 cm) laid in series (Fig. 4) constituted the experimental apparatus for reproducing mudflows. The first plane, set up with a 30° dip angle, was roughened by medium-fine sand glued on the surface; the second was smooth and horizontal to halt the flow. A Plexiglas box, having a facing gate and two triangular sides (7 × 14 × 12 cm), spaced out of 15 cm, was fixed on the top of the inclined plane and contained a 636.5 cm³ sample of soil before the test beginning. In order to minimize the material adhesion on the Plexiglas walls, the internal faces were lubricated with Teflon oil.

A digital camera placed above the experimental apparatus, at a 90° angle to the oblique plane, acquired photos of the running mud at a rate of 20 fps and permitted to accurately follow the movements of the soil after the manual lifting of the gate.

To analyze the effect of soil composition on the mudflow run-out three kinds of material were tested, all of them obtained removing or substituting the coarsest particles in the original soil (Fig. 2). According to the aforementioned definition of fine fraction, the compositions of the examined materials were:

- A – 100 % of fine fraction;
- B – 90.5 % of fine fraction and 9.5 % of sandy fraction (portion passing the n.7 ASTM sieve and retained on n.40 ASTM sieve);
- C – 57 % of fine fraction and 43 % of sandy fraction.

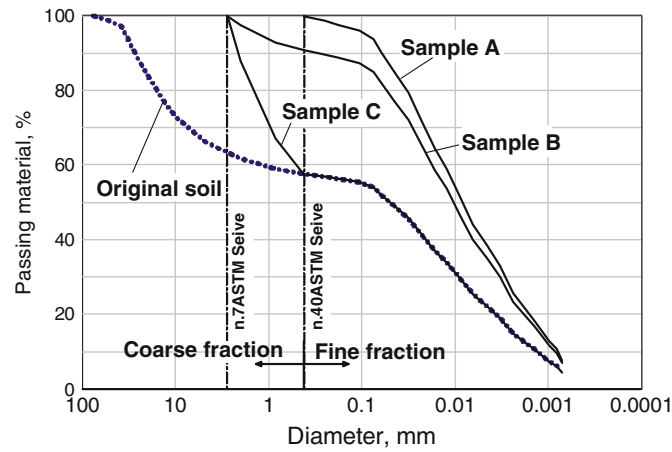


Fig. 2 Grain size distribution of sample collected in Tessina earth-flow and of recomposed samples

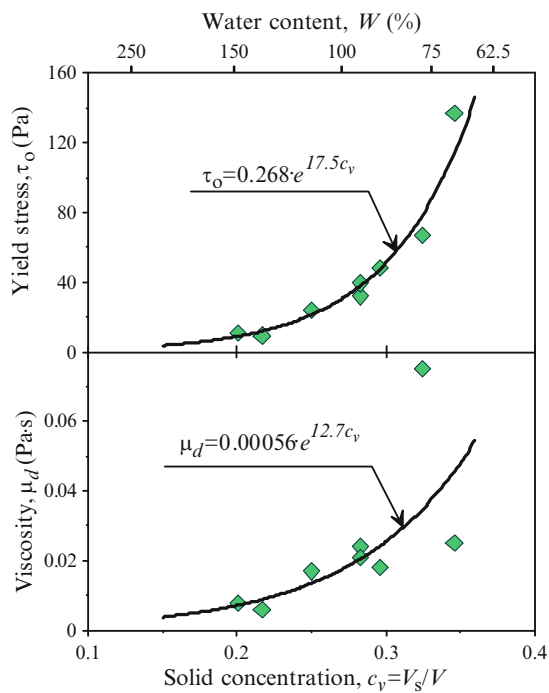


Fig. 3 Bingham yielding stress and viscosity versus solid concentration for the fine fraction of mud (data from two soils)

Since the water content affects both the matrix and global consistences, the samples A, B and C were prepared at a 54–70 % of the fine fraction or matrix water content W_f , defined as:

$$W_f = \frac{P_W}{P_{s,FF}} \cdot 100 \tag{4}$$

where P_W is the water weight and $P_{s,FF}$ the dried weight of the fine fraction.

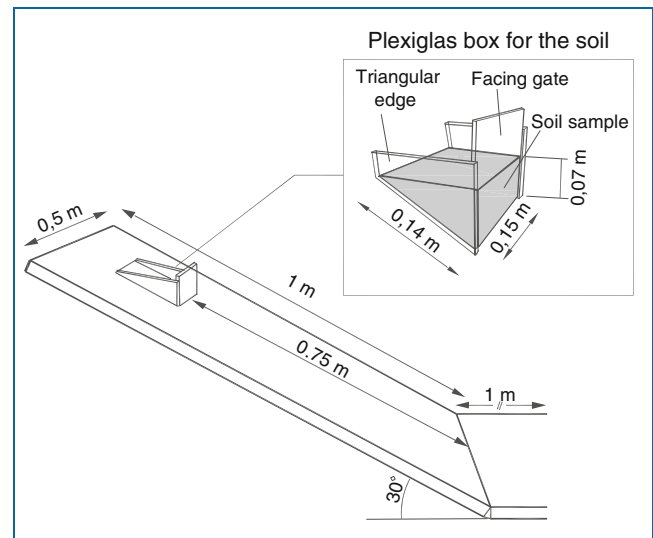


Fig. 4 Set up of equipment for mud-flow test

Experimental Results

The run-out of soil downhill the rough plane was always very rapid: after only 10–30'' the material reduced significantly its displacement rate. The Fig. 5 shows two typical final configurations of the mud tongue. The composition and solid concentration strongly affected the distance covered by the mass, varying from some centimetres to more that 75 cm.

The Fig. 6 shows the evolution of the tip maximum displacement and tongue spreading observed with time during the tests with sample A. Analogous trends were obtained with other mixtures, even if they are not here reported for brevity.

As noticed above, the phenomenon developed very quickly: it came to a halt in about 1 s. We can identify an initial stretch with a parabolic course and constant

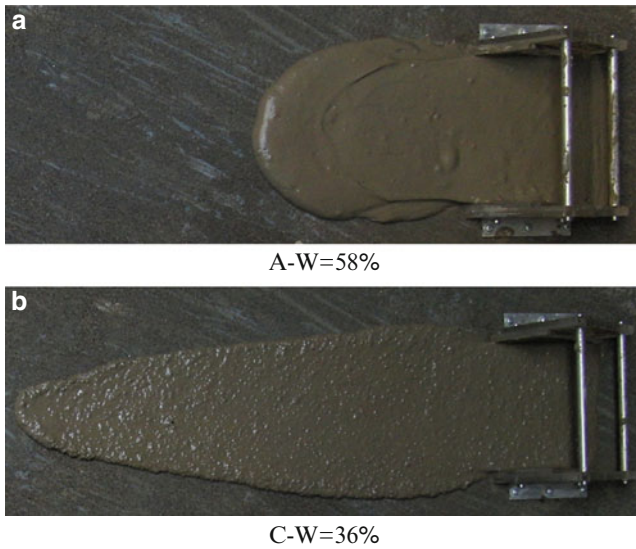


Fig. 5 Mud final configuration in two tests

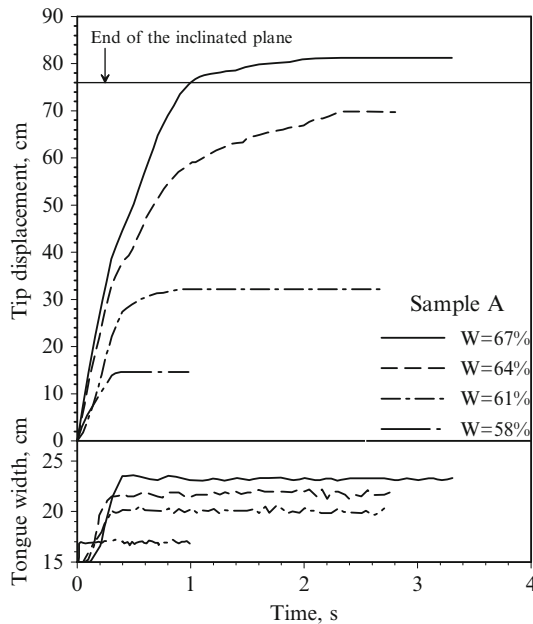


Fig. 6 Tip displacement and tongue width versus time in some tests with sample A

acceleration, then a deceleration phase up to the mass stop. The inflection point of the curve points out the instant (breaking time) at which the velocity is maximum. The lateral spreading showed the same trend, even if its variation is smaller, since the width of the tongue increased from 15 to 24–25 cm only.

Both the total displacement and the tongue width increased consistently with the water content, therefore greater is the water content more deformable is the soil mass. The breaking time also increased with water content.

In Fig. 7a the maximum tip displacements measured in the tests are related to the global water content W . An exponential law, also reported in Fig. 7a, may fit the results of tests for the same sample.

The fitting curve does not accurately interpolate the highest data for sample A, maybe because in this test the flow reached the end of the inclined plane and continued its path on the horizontal plane, as shown in Fig. 6.

Nevertheless, the correlation coefficients are always very good suggesting that the c_v controlled the flow as well as the viscosity parameters. Since this occurred for all the samples, we deduce that, even if the sample C contains a large amount of coarse particles, its flow was still affected by the viscosity of the material.

Supposing that the fitting curve has the same trend also at water contents higher than those tested, the fitting curves of sample C and B would be above the curve of sample A, indicating that, at the same water content, the sample A travels for the shortest distances and, vice versa, the sample C reaches the longest distances.

On the other hand, if we plotted the same data as a function of the fine fraction water content W_f (Fig. 7b), all the points lie in a narrow area. This indicates the key role of fine fraction consistence in determining the mixture behaviour, or, in other words, we may say that only this fraction controls the viscous response of soil. If the sandy fraction is there in small amount, it seems to be a constrain (sample B), but when it increases a lot, it behaves as a dead weight in the mixture, that increases the forces inducing the sliding along the plane without contributing to the viscosity of whole sample.

Unfortunately, it is not possible to draw any conclusions due to the small number of performed tests. Further investigation is required to elucidate the role of the composition of the soil in the behaviour of these processes.

Run-Out Mathematical Model

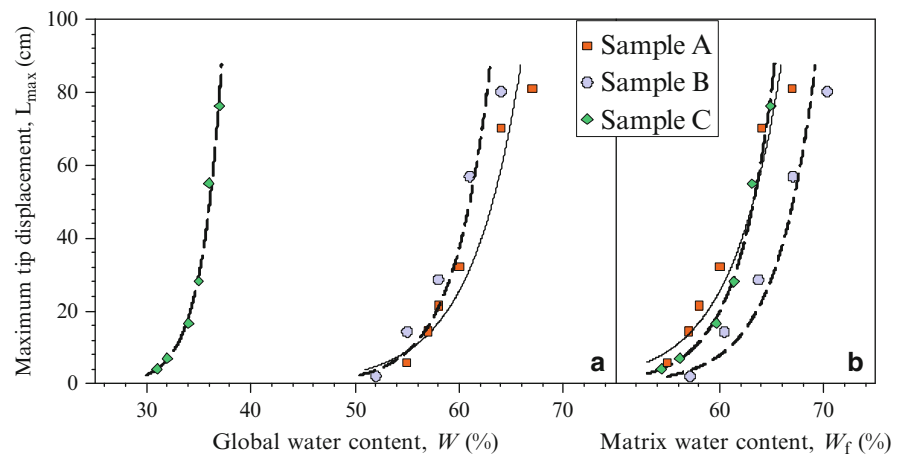
The depth-averaged model derived from the Biot–Zienkiewicz equations for non-linear materials and large deformation problems, i.e. the balance of mass and the balance of linear momentum for the mixture soil skeleton–pore fluid:

$$\frac{D^s \rho}{Dt} + \rho \operatorname{div} \mathbf{v}_s = 0 \quad (5)$$

$$\rho \frac{D^s \mathbf{v}_s}{Dt} = \rho \mathbf{b} + \operatorname{div} \boldsymbol{\sigma} \quad (6)$$

where D_s refers to a material derivative following the soil particles, ρ is the density of the soil and \mathbf{v}_s the velocity of soil

Fig. 7 Maximum tongue elongation in relation to the global water content (a) and the matrix water content (b)



skeleton, b the body forces and σ the Cauchy stress tensor. The integration of the above equations along the vertical axis taking into account the Leibniz's rule in a Lagrangian form is difficult, because the integration is not performed in a material volume. To avoid this difficulty the model refers to an equivalent 2D continuum in which each moving point represents a column of material, extending from the bottom to the free surface and travelling with the depth-averaged velocity.

This is not an exact Lagrangian formulation, because the moving points have no connection with material particles, but it can be denominated either 'quasi-Lagrangian' or arbitrary Lagrangian–Eulerian formulation. Its main advantage is a consistent reduction of the calculation time compared to a standard finite element code based on an Eulerian approach.

The depth-integrated relations derived from (5) and (6) in the quasi-Lagrangian formulation result:

$$\frac{\partial}{\partial x_j}(h\bar{v}_j) + \frac{\partial h}{\partial t} = 0 \quad j = 1, 2 \quad (7)$$

$$\rho \left[\frac{\partial}{\partial t}(h\bar{v}_j) + \frac{\partial}{\partial x_j}(h\bar{v}_i\bar{v}_j) \right] = \frac{\partial}{\partial x_j}(h\bar{\sigma}_{ij}) + t_j^A + t_j^B + \rho b_j h \quad (8)$$

where h is the landslide thickness, \bar{v}_j the depth averaged velocity and the terms t_j^A and t_j^B are the normal stress acting on the surface and bottom respectively.

The above results depend on the chosen rheological model, which, relating the stress tensor to the rate of strain tensor \mathbf{d} and, consequently, to the velocity field \mathbf{v}_s , influences the basal friction and depth integrated stresses $\bar{\sigma}_{ij}$. In the analysis of flow-like landslides the instantaneous flow at a given point may be studied as a uniform steady-state flow. Considering a 1D flow along a channel dip with a constant angle θ , the only non-null velocity component is $v_x = u$ parallel to the base, which varies along the axis

normal to the base. The mobilized shear stress related to a depth z is:

$$\tau = \rho g(h - z) \sin \theta \quad (9)$$

The general rheological law is:

$$\begin{aligned} \tau &= c + \sigma_n \tan \phi + \mu \frac{\partial v_x}{\partial x_3} \\ &= c + \rho g(h - z) \cos \theta \tan \phi + \mu \frac{\partial v_x}{\partial x_3} \end{aligned} \quad (10)$$

where c is the cohesion, σ_n the normal stress and ϕ the friction angle. By combining the three contributions in (10) it is possible to extract different rheological models (Newtonian model, frictional model, and so on).

In this study, we have considered the mud behaving as a Bingham fluid, since the Bingham model is suitable for flows with high water content and clay percentages greater than 10%. The rheological relations become:

$$\begin{aligned} \tau &= c + \mu \frac{\partial v_x}{\partial x_3} \quad \text{for } \frac{\partial v_x}{\partial x_3} \neq 0 \\ \tau &\leq c = \tau_c \quad \text{for } \frac{\partial v_x}{\partial x_3} = 0 \end{aligned} \quad (11)$$

where the second hypothesis implies that for $\tau < \tau_c$ there is no reciprocal motion and the material moves as a rigid block (plug zone).

Finally, (7) and (8) are solved with the method known as Smoothed Particle Hydro-dynamics or SPH, a particle method in which the flow domain is represented by nodal points that move with the flow and are scattered in space with no definable grid structure. Each nodal point carries scalar information, such as density, pressure, velocity components, etc. Interaction between the nodal points and interpolation from a set of N nodes to find the value of a

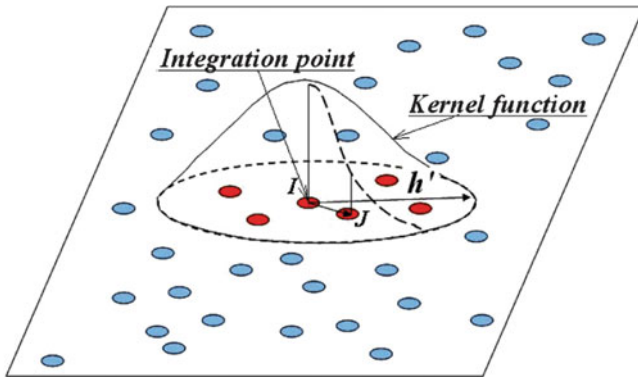


Fig. 8 Kernel function representation

particular quantity at an arbitrary point is obtained with a weighting function, also named the kernel function or smoothing function (Fig. 8).

For more details about the mathematical and numerical formulations, see also Pastor et al. 2008. Here, we remember only that an important numerical parameter of the model is the smoothing length h' , defined as the distance from each node where the weighting function becomes null (Fig. 8). Among the input data for the numerical, one has to assign the parameter h' or the no-size ratio $k = h'/i$, with i the initial spacing of integration point.

Numerical Tests

Figure 9 shows the mesh reproducing the experimental apparatus, formed by a grid with 10,547 nodes spaced of 0.1 m, and the initial position of the mud mass, modelled through 2,601 particles with an initial spacing $i = 0.005$ m.

Two experimental tests, i.e. the tests A–W = 57 % and A–W = 67 %, were simulated adopting viscosity parameters from (1) and (2).

Since the integration scheme is explicit, the time and space steps Δt e Δx have to satisfy the relation:

$$\Delta t \leq \Delta x / \sqrt{gh_{\max}} \quad (12)$$

where h_{\max} is the maximum value of h , equal to 7 cm in the artificial mudflows. Consequently, in addition to the rheological quantities, the parameters controlling the numerical model are the integration steps Δt e Δx and the smoothing length h' . To emphasize the effect of h' , we adopted fixed values for Δt e Δx , 0.006 s and 0.01 m respectively, and calibrated the value of k on the base of test A–W = 67 %.

Figure 10 compares the tip displacement vs. time curves calculated by the model in tests with $k = 0.5$, 2 and 10 with the experimental data. Since the greater is k , and the

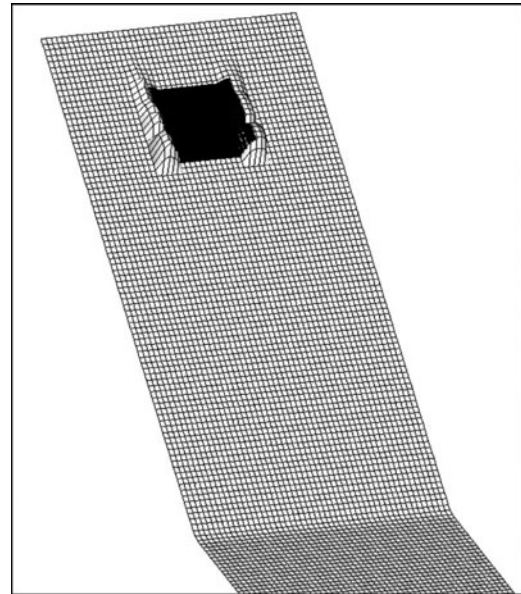


Fig. 9 Initial particles configuration and terrain mesh for the numerical model

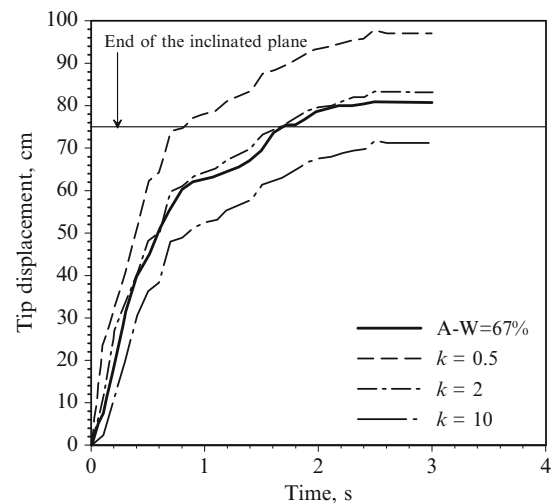


Fig. 10 Effect of the smoothing length on the run-out of mudflows: comparison with data from test A–W = 67 %.

corresponding h' , the greater is the number N of nodes utilized for the interpolation by the kernel function: consequently, with high values of k the nodes result more bonded one to each other and, consequently, the mass resulted more constrained and covered a smaller maximum distance, like it is evident in Fig. 10.

For k equal to 2 we find the best correspondence between experimental and numerical curves: both the curves reach the complete stop in about 2 s and the numerical predicted maximum displacement is 84 cm, against the experimental value of 77.2 cm.

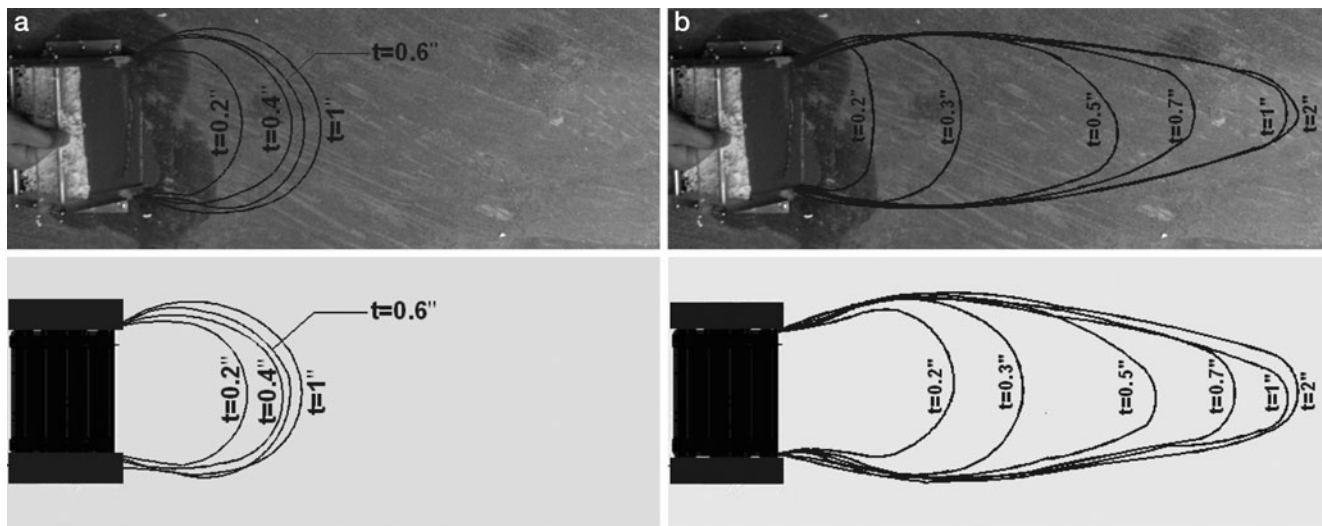


Fig. 11 Tongue configurations in the experimental and numerical tests for (a) A-W = 57 % and (b) A-W = 67 %.

The numerical data deviated from the experimental one only at the beginning of the process when the simulated flow is faster than the experimental one.

Finally, Fig. 11 compares the experimentally observed and numerically predicted configurations of the mudflow at different instants during the reference tests. The phenomenon is properly identified and the mud path and the final tongue form are in agreement with experimental observations.

Conclusion

The paper presents some experimental data on small laboratory mudflow performed with various soil composition and solid concentration: the results highlight the crucial role of fine fraction in controlling the viscosity and the overall behaviour of these phenomena.

The adopted SPH depth-averaged model, which considers the mud as a Bingham fluid, proved to be able to reproduce the observed experimental behaviour as shown by the good agreement between the experimental and numerical run-out distance, lateral spreading and development in time of the process.

Acknowledgements This paper is a part of the research Project MoVeMit financed by the funding of the “Fondazione Cassa di Risparmio di Verona, Vicenza, Belluno e Mantova”. The authors wish thanking also the “Fondazione Angelini” of Belluno and the CNR-IRPI of Padova, which covenant this activity research.

References

- Cola S, Calabrò N, Pastor M (2008) Prediction of the flow-like movements of Tessina landslide by a SPH model. In: Proceedings of the 10th international symposium on landslide and engineering slopes, Xi'an, China, vol. 1. Taylor & Francis, The Netherlands, pp 647–653
- Coussot P, Piau JM (1994) On the behaviour of fine mud suspensions. *Rheol Acta* 33:175–184
- Gingold RA, Monaghan JJ (1977) Smoothed particle hydro-dynamics: theory and application to non-spherical stars. *Mon Not R Astron Soc* 81:375–389
- Hutter K, Koch T (1991) Motion of a granular avalanche in an exponentially curved chute: experiments and theoretical predictions. *Phil Trans R Soc Lond* 334:93–138
- Laigle D, Coussot P (1997) Numerical modeling of mudflows. *J Hydraul Eng, ASCE* 123(7):617–623
- Lucy LB (1977) A numerical approach to testing of fusion process. *Astron J* 82:1013–1024
- Major JJ, Pierson TC (1992) Debris flow rheology: experimental analysis of fine-grained slurries. *Water Resour Res* 28:841–857
- Pastor M, Haddad B, Sorbino G, Cuomo S, Drempetic V (2008) A depth integrated coupled SPH model for flow-like landslides and related phenomena. *Int J Numer Anal Meth Geomech* 33:143–172
- O'Brien JS, Julien PY (1988) Laboratory analysis of mudflow properties. *J Hydraul Eng, ASCE* 110:877–887
- Savage SB, Hutter K (1991) The dynamics of avalanches on granular materials from initiation to runout. Part I: *Anal. Acta Mech* 86, Madrid 2001, pp 201–223